Hindawi
Structural Control and Health Monitoring
Volume 2023, Article ID 6665803, 16 pages
https://doi.org/10.1155/2023/6665803

Research Article

Development of a High-Sensitivity and Adjustable FBG Strain Sensor for Structural Monitoring

Heying Qin,[1,2] Chunde Li,[1,2] Jianqiang Zhu,[1,2] Boguang Luo,[1,2] and Feng Fu [1,3]

[1]*College of Civil Engineering and Architecture, Guilin University of Technology, Guilin 541004, China*
[2]*Guangxi Key Laboratory of Geotechnical Mechanics and Engineering, Guilin University of Technology, Guilin 541004, China*
[3]*Department of Engineering, School of Science & Technology, City, University of London, Northampton Square, London EC1V 0HB, UK*

Correspondence should be addressed to Feng Fu; feng.fu.1@city.ac.uk

Received 30 June 2023; Revised 9 October 2023; Accepted 6 November 2023; Published 15 November 2023

Academic Editor: Fabio Casciati

In this paper, a new fiber Bragg grating (FBG) strain sensor with adjustable sensitivity is invented. The sensitivity adjustment, strain sensing, and temperature compensation principles of the sensor and the corresponding formulae are developed. The prototype sensor specimen is developed, and a series of tests are performed to investigate its strain sensitivity and temperature compensation characteristics. The results show that the strain sensitivity of the sensor can be adjusted effectively by the correspondent L/L_{FBG} parameter, with an acceptable discrepancy within ±5% of the theoretical value. The linearity, repeatability, and hysteresis were analyzed, and the errors were 0.98%, 1.15%, and 0.09%, respectively, with excellent performance. When the temperature difference was 20°C, through temperature compensation calibration, the error between the monitored strain and the actual strain was within 5% after temperature compensation correction, showing that this new type of FBG strain sensor can meet the strain monitoring needs of various engineering structures and provide reliable data acquisition.

1. Introduction

With the rapid development of structural health monitoring (SHM) [1–5], the application of new materials and advanced processes, the structural system becomes increasingly complex, and the traditional structural monitoring sensors can hardly meet the long-term monitoring needs. However, due to its small size, light weight, good stability, strong antiinterference, long-distance transmission, and other significant advantages of fiber Bragg grating (FBG) [6–11], it applies for health monitoring of structural performance widely and in-depth, for example, online monitoring of transformers [12], sliding warning of slopes [13], long-term health monitoring of roads [14], corrosion rate monitoring of prestressed structures [15], and real-time monitoring of the full corrosion process of reinforcement in concrete structures [16], monitoring of bridge structures during proof load testing (PLT) [17], and other structural health monitoring studies [18–21]. Strain is an important performance parameter of engineering structures and is closely related to the internal forces and deformation of the structure, so strain monitoring is one of the most important means of obtaining the health status of engineering structures. As a sensor for strain monitoring, the strain sensitivity of a fiber Bragg grating is an important indicator of its performance, and the larger the coefficient, the higher the monitoring accuracy. By improving the material properties of fiber Bragg gratings, their sensitivity coefficients can be improved. Sridevi et al. [22] developed an etched sensor with a strain sensitivity of 5.5 pm/$\mu\varepsilon$ by coating graphene on fiber Bragg gratings; also for etched sensors, Oliveira et al. [23] fused polymer ZEONEX-480R fiber Bragg gratings with silicon fibers as a coating for FBGs, increasing their strain sensitivity to 13.4 pm/$\mu\varepsilon$. In addition, some scholars have investigated FBG strain sensors etched with different material coatings [24, 25], all achieving high sensitivity. These etching techniques mainly involve coating the fiber Bragg grating, which in turn improves the strain sensitivity of the sensor by

changing the effective refractive index of the fiber Bragg grating, but the difficulty and accuracy of the material fabrication limit their prevalence for monitoring engineering structures. A simple and straightforward way to monitor strain in fiber Bragg gratings is to adhere the bare fiber Bragg grating to the structure to be measured or to embed the fiber Bragg grating in a polymer composite to achieve intelligent monitoring of the structure [26, 27], at which point the strain sensitivity of the bare fiber Bragg grating is approximately 1.21 pm/$\mu\varepsilon$, as the resolution and accuracy of commonly used demodulators are 1 pm and ±5 pm, respectively, the resolution and accuracy of the bare fiber Bragg grating strain sensor are 0.8 $\mu\varepsilon$ and ±4 $\mu\varepsilon$, which is difficult to apply to the monitoring of small strains (less than 20 $\mu\varepsilon$). Changing the mechanical structure of the sensor can also improve its sensitivity coefficient. Li et al. [28] used an adhesive to fix the fiber Bragg grating to the substrate and used the lever principle to amplify the deformation of the measured component sensed by the fiber Bragg grating to increase the strain sensitivity of the sensor to 6.2 pm/$\mu\varepsilon$; [29] applied the principle of concentrated sensitivity enhancement and developed a sensor with a strain sensitivity of 10.84 pm/$\mu\varepsilon$ based on a flexible hinge structure; Peng's team combined the above two sensitivity enhancement principles and developed a FBG sensor with a strain sensitivity of 11.49 pm/$\mu\varepsilon$ [30]. The FBG sensor developed by Nawrot et al. [31] based on the symmetrical double cantilever structure increases the strain sensitivity by more than 30 times and can be used for small strain monitoring of structures. Due to the strain-temperature cross-sensitivity of fiber Bragg gratings, the necessary temperature compensation should be applied to FBG strain sensors when there is a temperature change [32–36].

Building structures are subjected to harsh service environments such as wind, vehicles, seismic, sun, and rain. When strain monitoring is carried out by means of direct paste [26, 27] or indirect paste [28], the fiber Bragg grating is prone to fall off after a long period of environmental action, making it difficult to achieve long-term health monitoring, and direct paste [26, 27] is more difficult to produce and install, while indirect paste [28] has a certain impact on the structural force itself due to the greater stiffness of the sensor itself. The use of the hinge [29, 30] method for sensors in complex and vibrating engineering structures presents a challenge due to the thin and fragile nature of the hinge, resulting in a low survival rate. Such structures, including bridge engineering and long-span space engineering, are comprised of various components, each with different stress states and strain ranges. The use of a sensor with a fixed and nonadjustable sensitivity coefficient [26–30] is not feasible for monitoring different structural parts simultaneously, as it would require an excessive number of sensors and affect mass production and application. In order to improve the production efficiency and meet the static and dynamic measurement of multiple parts of the structure, as well as to avoid excessive sensor stiffness affecting structural forces, long-term monitoring, and other factors, this paper proposes a high-sensitivity and adjustable FBG strain sensor, and the structure of the sensor is designed based on the principles of strain monitoring and temperature compensation: the stiffness of the sensor is close to that of the fiber grating itself, which is low and avoids affecting the force of the measured structure and improves the monitoring accuracy; it adopts the screw fixing method, which is easy to be installed on all kinds of structural components in the harsh service environment; it adjusts the ratio between the distance L of the two support fixing tubes and the distance L_{FBG} of the grating pasting point, i.e., L/L_{FBG}, so as to realize the sensitivity adjustability, which applies to the large amount of ranges as well as the monitoring of high accuracy; and it adopts the reference grating method to carry out the temperature compensation of the sensor to eliminate the temperature changes in the harsh service environment on the sensor monitoring performance. On the basis of theoretical and structural design, a series of verification tests were designed to verify the performance of the sensor, such as sensitivity adjustment, linearity, repeatability, hysteresis, and temperature compensation. The excellent sensitivity-adjustable FBG strain sensor proposed in this paper can provide flexible monitoring means and technical support for various complex engineering structures and their various components.

2. Algorithm of FBG Monitoring

A FBG is an optical fiber in which the index of refraction within the core of the fiber changes along its length, from high-index to low-index. The modulation of the refractive index causes an FBG to act like a mirror that reflects certain wavelengths and transmits others. According to the coupled mode theory, its central wavelength λ_B is determined by the refractive index n_{eff} of the core and the grating period Λ is expressed as follows:

$$\lambda_B = 2n_{\mathrm{eff}}\Lambda. \tag{1}$$

It can be seen from equation (1) that the variation of the center wavelength of the grating is positively correlated with the refractive index of the core and the grating period. In practical engineering applications, the strain sensor based on FBG is only affected by stress and temperature, which cause the center wavelength of the fiber Bragg grating to change.

2.1. FBG Strain Monitoring. When the fiber Bragg grating is subjected to axial strain at a constant temperature, the axial strain will change its period and the photoelastic effect will change its core refractive index. At this point, the relationship between the central wavelength shift $\Delta\lambda_B$ of the fiber Bragg grating and its strain $\varepsilon_{\mathrm{FBG}}$ is [37, 38]:

$$\Delta\lambda_B = (1 - p_e)\lambda_B \cdot \varepsilon_{\mathrm{FBG}}, \tag{2}$$

where p_e is the effective elasto-optic coefficient, which is generally 0.22 for common quartz fiber; and λ_B is the center wavelength of the grating.

2.2. FBG Temperature Compensation. The main reasons for the change in the center wavelength of the fiber Bragg grating are caused by the temperature variations, including the thermal expansion effect of the fiber material, the thermo-optical effect, and the photoelastic effect caused by the thermal stress inside the fiber. Among them, the thermal expansion will cause the grating period to change, the thermo-optical effect will cause the effective refractive index of the grating to change, and the photoelastic effect coefficient is neglected because it is much smaller than the thermal expansion effect and the thermo-optical effect coefficient.

When the bare fiber Bragg grating is only affected by the temperature change, the central wavelength shift of the fiber Bragg grating is as follows [39]

$$\Delta\lambda_B = (\xi_F + \alpha_F)\lambda_B \Delta T. \tag{3}$$

When the bare fiber Bragg grating is affected by strain and temperature at the same time, the central wavelength shifts $\Delta\lambda_B$ of the FBG obtained by simultaneous (2) and (3) is

$$\Delta\lambda_B = (1 - P_e)\lambda_B \varepsilon_{\mathrm{FBG}} + (\xi_F + \alpha_F)\lambda_B \Delta T, \tag{4}$$

where ΔT is the temperature variation and ξ_F and α_F are the coefficients of thermal-optic and thermal expansion for optical fibers, with values of approximately $\xi_F = 6.55 \times 10^{-6}$ and $\alpha_F = 0.55 \times 10^{-6}$, respectively.

When the fiber Bragg grating is pasted on the substrate material, as the thermal expansion coefficient of the substrate material is different from that of the fiber Bragg grating, the fiber Bragg grating will be stretched or compressed simultaneously by the thermal expansion effect of the substrate material. If this force due to the different thermal expansion coefficients is approximated as an axial force, then the axial strain of the fiber Bragg grating by this force is $\varepsilon_{\mathrm{FBG}} = (\alpha_M - \alpha_F)\Delta T$.

When the fiber Bragg grating is pasted onto the substrate material and subjected to temperature variation, only, the center wavelength shift of the fiber Bragg grating can be obtained from equation (4) as follows:

$$\Delta\lambda_B = [(1 - P_e)(\alpha_M - \alpha_F) + (\xi_F + \alpha_F)]\lambda_B \Delta T, \tag{5}$$

where α_M is the coefficient of thermal expansion of the substrate.

When the fiber Bragg grating is bonded to the substrate material and is affected by the strain and temperature at the same time, the central wavelength shift of the fiber Bragg grating is obtained from equations (4) and (5).

$$\Delta\lambda_B = (1 - P_e)\lambda_B \varepsilon_{\mathrm{FBG}} + [(1 - P_e)(\alpha_M - \alpha_F) + (\xi_F + \alpha_F)]\lambda_B \Delta T. \tag{6}$$

As can be seen from equation (6), when coupling a fiber Bragg grating to a substrate to measure its strain, the change in temperature and the difference in the coefficient of thermal expansion between the fiber Bragg grating and the substrate material should be excluded from the amount of change in the central wavelength, otherwise it will result a large error in the measured strain. Therefore, the temperature compensation of the FBG is needed. The FBG strain sensor in question is made of stainless steel and has a coefficient of thermal expansion of $\alpha_M = 1.5 \times 10^{-5}$.

3. Design of the New FBG Strain Sensor with Adjustable Sensitivity

The section view of the new FBG strain sensor with adjustable sensitivity is shown in Figure 1. The sensor consists of two fixed tubes, two clamping rods, springs, protective tubes, and an optical fiber engraved with strain gratings and temperature-compensated gratings. Considering the influence of the stiffness and paste of the fiber grating on the sensitivity and the deviation of the temperature on the strain monitoring, the strain grating on the optical fiber is placed in the middle of the two clamping rods, and the temperature-compensated grating is placed in the clamping rod at one end. Among them, the L segment is covered with a bare fiber protection tube. After the two ends of the L segment are sealed, the optical fiber and the temperature-compensated grating are attached in the groove of the clamping rod using an adhesive, and then the optical fiber is extended to the outside of the fixed tube. Then the spring protected with a protective sleeve is assembled, both ends are sleeved outside the clamping rod, and the spring needs to be preloaded during assembly to make the optical fiber in a tightening position; the assembly of the clamping rod and the bearing fixed tube at both ends is connected by internal and external threads; finally, the optical fibers at both ends run through the clamping rod and the support fixed tube in turn. Among them, the optical fiber jumper protection tube is set outside the two support fixed tubes to protect the optical fiber and install it on the measured object through the support. After the processing of the whole structure is completed, the suspended part of the fiber Bragg grating is protected by glue. The stiffness of this FBG strain sensor is very small and is essentially equivalent to that of a fiber Bragg grating. When the sensor is installed on the specimens, the support fixed tube slides with the displacement of the specimens, causing the wavelength of the strain grating changes, and the wavelength change of the temperature compensation grating is only affected by temperature.

Let the distance between the optical fibers at the two ends of the strain grating at the attachment point of the clamping rod be L_{FBG}, and the distance between the midpoints of the two fixed tubes be L. When the fixed tubes slide with the strain of the specimens to be measured, the stiffness of the optical fibers is much less than that of the clamping rod and the fixed tube, so the elongation of the optical fibers and the fixed tube can be presumed to be the same, i.e., $\Delta L = \Delta L_{\mathrm{FBG}}$. Let the strain of the object to be measured be ε, and the strain of the strain grating be $\varepsilon_{\mathrm{FBG}}$. The ratio between the two is

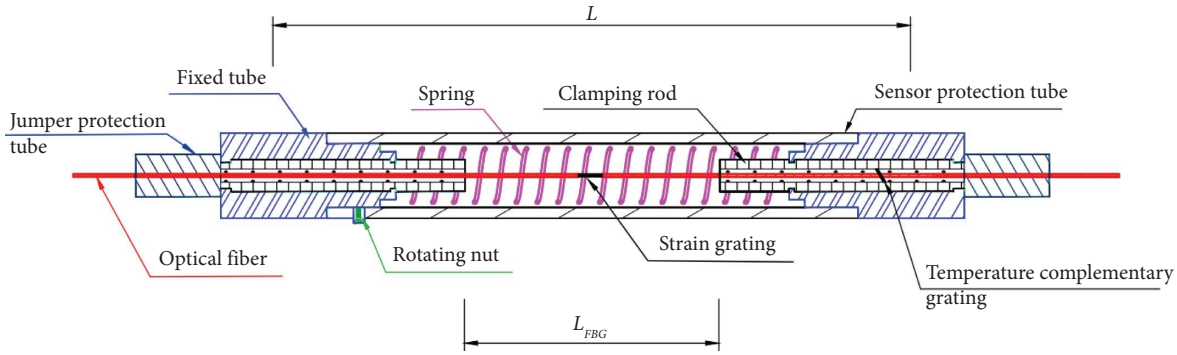

Figure 1: FBG sensor structure diagram.

$$\frac{\varepsilon_{\mathrm{FBG}}}{\varepsilon} = \frac{\Delta L_{\mathrm{FBG}}/L_{\mathrm{FBG}}}{\Delta L/L} = \frac{\Delta L_{\mathrm{FBG}} * L}{\Delta L * L_{\mathrm{FBG}}} = \frac{L}{L_{\mathrm{FBG}}}. \tag{7}$$

From the above equation, the ratio of the strain $\varepsilon_{\mathrm{FBG}}$ of the strain grating to the strain ε of the object to be measured is equal to the ratio of the distance between the midpoints of the two fixed tubes and the distance between the attachment points of the fibers at the ends of the strain grating.

The relationship between the shift of the central wavelength of the fiber Bragg grating and the strain ε of the measured object without the influence of temperature can be obtained by combining equations (2) and (7) as follows:

$$\Delta\lambda_B = \frac{L}{L_{\mathrm{FBG}}} \cdot (1 - p_e)\lambda_B \cdot \varepsilon. \tag{8}$$

From equation (2), the strain sensitivity coefficient of the bare grating is $K_\varepsilon = (1 - P_e)\lambda_B$ for universal FBG sensors from equation (8) for the new sensor, the strain sensitivity coefficient of the strain sensor is $K_{\varepsilon-S} = (1 - p_e)\lambda_B L/L_{\mathrm{FBG}}$. Comparing the two sensitivity coefficients, it can be seen that changing the ratio between L and L_{FBG} can adjust the sensitivity of the strain sensor. When the strain ε of the measured object is less than the limit strain $\varepsilon_{\mathrm{FBG}}$ of the strain grating, the sensitivity needs to be increased to make $L > L_{\mathrm{FBG}}$; when the strain ε of the measured object is greater than the limit strain $\varepsilon_{\mathrm{FBG}}$ of the strain grating, it is necessary to expand the monitoring range and reduce the sensitivity. By extending the clamping rod, the distance between the two fixed tubes is reduced, and the two sticking points of the optical fiber in the groove of the clamping rod are moved outward, so that $L < L_{\mathrm{FBG}}$ can be achieved. In practice, L can be determined according to the installation space of the measured object and the required range. According to equation (8), L_{FBG} can be determined theoretically to determine the distance between the two clamping rods; this is the principle of the sensor with adjustable sensitivity.

When the sensor is affected by both strain and temperature, the relationship between the two can be obtained by combining equations (6) and (7) as follows:

$$\Delta\lambda_B = \frac{L}{L_{\mathrm{FBG}}}(1 - p_e)\lambda_B \cdot \varepsilon + [(1 - P_e)(\alpha_M - \alpha_F) + (\xi_F + \alpha_F)]\lambda_B \Delta T. \tag{9}$$

Let the temperature sensitivity coefficient of the strain grating be $K_{T-S} = [(1 - P_e)(\alpha_M - \alpha_F) + (\xi_F + \alpha_F)]\lambda_B$, then equation (9) can be simplified as follows:

$$\Delta\lambda_B = K_{\varepsilon-S}\varepsilon + K_{T-S}\Delta T, \tag{10}$$

where the temperature variation ΔT can be obtained by the temperature compensation grating. Let the initial central wavelength of the temperature compensation grating be $\lambda_{B,T}$, the central wavelength shift be $\Delta\lambda_{B,T}$, and the temperature sensitivity coefficient be $K_{T-T} = [(1 - P_e)(\alpha_M - \alpha_F) + (\xi_F + \alpha_F)]\lambda_{B,T}$. From equation (5): $\Delta T = \Delta\lambda_{B,T}/K_{T-T}$, substitute into equation (10):

$$\Delta\lambda_B = K_{\varepsilon-S}\varepsilon + K_{T-S}\Delta T = K_{\varepsilon-S}\varepsilon + K_{T-S}\frac{\Delta\lambda_{B,T}}{K_{T-T}}, \tag{11}$$

where the strain sensitivity coefficient $K_{\varepsilon-S}$ and the temperature sensitivity coefficient K_{T-S} of the strain grating and the temperature sensitivity coefficient K_{T-T} of the temperature compensated grating can be obtained by the calibration of the sensor. This is the principle of temperature compensation of the strain sensor using the temperature reference grating method.

At present, the key effort in this paper is to enhance the strain sensitivity coefficient by reducing the stiffness of the fiber Bragg grating paste section of the conventional FBG strain sensor, but the degree of stiffness reduction is limited, and once the sensor is processed, the sensitivity coefficient is fixed. The stiffness of the FBG strain sensor developed in this paper has been reduced to be equal to the stiffness of the fiber Bragg grating. The stiffness of the fiber Bragg grating is almost negligible compared to the stiffness of the measured structure, and the sensitivity adjustment can therefore be

achieved by changing the ratio between L and L_{FBG}. Even after the sensor is processed, the distance L can be changed to achieve the sensitivity adjustment. Due to the essential difference in structural design, the FBG strain sensor developed in this paper has the following remarkable characteristics compared with the conventional FBG strain sensor, as shown in Table 1:

4. Prototype Testing of the New FBG Strain Sensor

4.1. Sensor Material and Structural Parameters. According to the structure diagram in Figure 1, the material selection for each part of the sensor is as follows: The clamping rod is an important part of the fiber Bragg grating. Based on the research results of the team on the bonding performance of optical fiber, the spacing should not be less than 40 mm [40], the diameter is 4~8 mm, and considering the monitoring condition, the material selected was 304 stainless steel. The support fixed tube is fixed to the measured component by clamping or welding methods. Combined with the size of the common support, the length of 25 mm, the wall thickness of 3 mm, and the substrate of 304 stainless steel pipes are selected and its inner diameter is matched with the clamping rod. The compression spring adopts 65 Mn spring steel with good elasticity and high fatigue strength. The protective tube is made of stainless steel circular tube adapted to support the fixed tubes; the optical fiber jumper protection tube is made of 304 stainless steel circular tubes, 25 mm in length, 2 mm in wall thickness, and 7 mm in outer diameter.

It can be seen from equation (8) that the theoretical strain sensitivity coefficient $K_{\varepsilon-S}$ of the FBG strain sensor is positively correlated with L/L_{FBG}, so the sensitivity coefficient can be adjusted by controlling the value of L/L_{FBG}. In order to verify the reliability of this method, the distance L between the midpoint of the fixed tube and the distance L_{FBG} between the optical fiber sticking points is taken as the change parameter. According to the fact that the total length of the specimen is 137 mm, L is 70 mm~80 mm, and L_{FBG} is 40 mm~50 mm, the specific parameters are shown in Table 2:

Based on the above materials and parameters, the physical diagram of the developed FBG sensor is shown in Figure 2.

4.2. Strain sensitivity Test of Strain Grating. Sensitivity is an important performance index of the sensor, reflecting its sensitivity to external stress and strain. In general, there is a serious constraint relationship between sensitivity and monitoring range. According to practical engineering applications, the sensitivity should be improved as much as possible when a certain monitoring range is guaranteed. The specific steps of the strain sensitivity test of the FBG strain sensor are as follows:

(1) In the constant ambient temperature of 20°C, the strain sensor is fixed on the displacement platform, and the fiber grating demodulator is connected with the jumper. (2) Use the vernier caliper to check L, clear the displacement meter, and read the initial center wavelength value λ_B of the strain grating from the software system; (3) Increase from 0 $\mu\varepsilon$ to 3000 $\mu\varepsilon$ at a rate of 600 $\mu\varepsilon$ per step displacement and perform the grading test. The displacement of each step is held for 5 minutes and the central wavelength reading λ_i of each step strain grating is recorded. (4) The strain unloading is carried out with a displacement of 600 $\mu\varepsilon$ per stage, and the unloading process is the same as that of (3), forming a cycle; (5) Repeat steps (3)~(4) twice. The accuracy of the displacement meter used in the test is 0.001 mm, the accuracy of the displacement table is 0.69×10^{-3} mm, and the wavelength resolution of the fiber grating demodulator is 0.1 pm. The device is shown in Figure 3. Taking the central wavelength shift $\Delta\lambda$ of each level of the strain grating as the vertical coordinate and the strain value as the horizontal coordinate, the diagram is drawn and linearly fitted. The experimental results are shown in Figure 4.

Figure 4 shows that the wavelength shift $\Delta\lambda$ of the strain grating is positively correlated with the strain ε during loading and unloading, with a linear correlation coefficient of 99.97% or more. The slope of the curve is the strain sensitivity coefficient $K_{\varepsilon-S}$. The average value of the strain sensitivity coefficient for the six positive and reverse itineraries was taken as the test value of the strain sensitivity coefficient $K_{\varepsilon-S,M}$ and compared with its theoretical value, and the data were compiled as shown in Table 3.

According to Table 3, as the L/L_{FBG} value increases, the strain sensitivity coefficient of the sensor increases proportionally, and the error of its theoretical value is very small, all within 5%. The error between the experimental value and the theoretical value of the sensitivity coefficient of S_1, S_2, and S_3 sensors is −2.08%, 0.10%, and −4.84%, respectively. The experimental results show that the sensitivity coefficient can be adjusted by changing the value of L/L_{FBG}.

In order to verify the real performance of FBG strain sensors, the linearity, repeatability, and hysteresis of the strain sensitivity coefficients are analyzed using the S_2 sensor as an example.

4.2.1. Linearity analysis of the Strain Sensitivity Coefficient $K_{\varepsilon-S}$. The linearity of the FBG sensor strain sensitivity reflects the degree of linear correlation between the test value and the linear fitting curve value during the sensitivity calibration. The smaller the linear error, the greater the correlation, indicating better linearity.

Let the wavelength shift corresponding to each strain level be the average value $\Delta\overline{\lambda}_i$ of the three repeated test values, where $i = 1 \sim 6$; the least square method is used to linearly fit the $\Delta\overline{\lambda}_i$ of the positive and reverse itineraries, and the fitting curve is shown in Figure 5.

The $\Delta\overline{\lambda}_i$ and its fitting value $\Delta\overline{\lambda}_{i,m}$ and the error $\Delta\overline{\lambda}_i - \Delta\overline{\lambda}_{i,m}$ between them are obtained under the 6 levels of strain for positive and reverse itineraries, as shown in Table 4.

Assuming that $\Delta\overline{\lambda}_i$ corresponding to the maximum strain 3000 $\mu\varepsilon$ is $\Delta\overline{\lambda}_{max}$ and $\Delta\overline{\lambda}_i$ corresponding to the minimum strain 0 $\mu\varepsilon$ is $\Delta\overline{\lambda}_{min}$, the sensitivity linear error can be expressed as follows:

Table 1: Comparison of the characteristics of the FBG strain sensors designed in this paper with those of conventional FBG strain sensors.

Comparative items	The FBG strain sensors designed in this paper	Conventional FBG strain sensors
Accuracy of monitoring	The structure has low stiffness and is easily deformed. Whether monitoring large or small strains, the monitoring sensitivity and measurement accuracy are high	When used for small strain measurements, the monitoring accuracy is low
Measurement range	The adjustable range is large, which is not only suitable for strain monitoring with a smaller limit strain than the fiber grating itself, but also suitable for strain monitoring with a larger limit strain than the fiber grating itself	It is difficult for the range of the external sensor to exceed the ultimate strain of the fiber grating itself
Whether or not it affects the forces on the member under test	The stiffness of the sensor is very small, close to the stiffness of the fiber grating itself, and does not change the stress state of the measured component	Sensors are used for the monitoring of small stress components, which affect the stress state of the measured components
Quality of installation	The support can be fixed with a small force when it is installed. It can be clamped or welded. The installation is convenient and reliable, and the quality is easy to guarantee	As the sensor has a certain stiffness, it is possible to produce deformation or cracks in the support after use
Initial error	There is a pretension after fabrication of the fiber Bragg grating, and there is no initial error for fabrication and installation	It is possible to produce initial errors

Table 2: FBG sensor number and parameters.

Sensor number	Fixed length L (mm)	Paste length L_{FBG} (mm)	L/L_{FBG}	Initial center wavelength (nm)	Theoretical value of strain sensitivity (pm/$\mu\varepsilon$)
S_1	70	50	1.40	1543.7408	1.686
S_2	80	50	1.60	1543.6654	1.926
S_3	70	40	1.75	1543.6677	2.107

Figure 2: FBG sensor physical image.

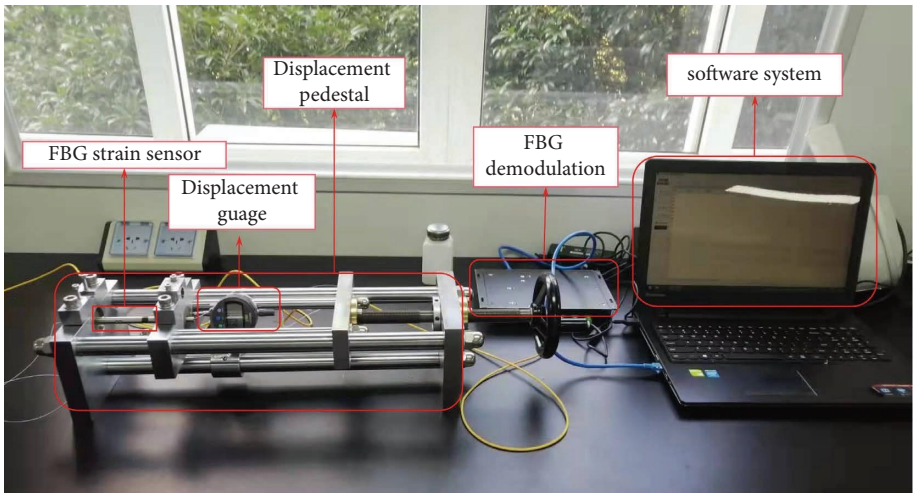

Figure 3: Strain sensitivity test device.

$$\delta = \frac{\max\left(\Delta\overline{\lambda}_i - \Delta\overline{\lambda}_{i,m}\right)}{\Delta\overline{\lambda}_{\max} - \Delta\overline{\lambda}_{\min}} \times 100\%. \tag{12}$$

It can be seen from the data in Table 4 that $\max(\Delta\overline{\lambda}_i - \Delta\overline{\lambda}_{i,m}) = 56.35$ pm, $\Delta\overline{\lambda}_{\max} = 5759.2$ pm, and $\Delta\overline{\lambda}_{\min} = 0.67$ pm, and the sensitivity linearity error $\delta = 0.98\%$ can be obtained by substituting it into equation (12), indicating that the FBG strain sensor has good linearity.

4.2.2. Repeatability analysis of the Strain Sensitivity Coefficient $K_{\varepsilon-S}$. The repeatability of the FBG sensor strain sensitivity determines whether it can complete the monitoring task and ensure the accuracy of the monitoring data. It reflects the degree of deviation in wavelength shift caused by the same strain in different paths during sensitivity calibration. The smaller the repeatability error is, the higher the stability of the monitoring will be.

Assuming that the three repeated test values of the wavelength variation corresponding to the same strain in different orders are $\Delta\lambda_{R-\mathrm{mn}}$ and the average value is $\Delta\overline{\lambda}_{R-n}$, where $m = 1 \sim 3$, $n = 1 \sim 6$, plot the sensor strain grating K versus time, as shown in Figure 6.

From Figure 6, $\Delta\lambda_{R-\mathrm{mn}}$ and $\Delta\overline{\lambda}_{R-n}$ can be obtained, then the standard deviation of the sensitivity value of the sensor for three repeated tests can be expressed as follows:

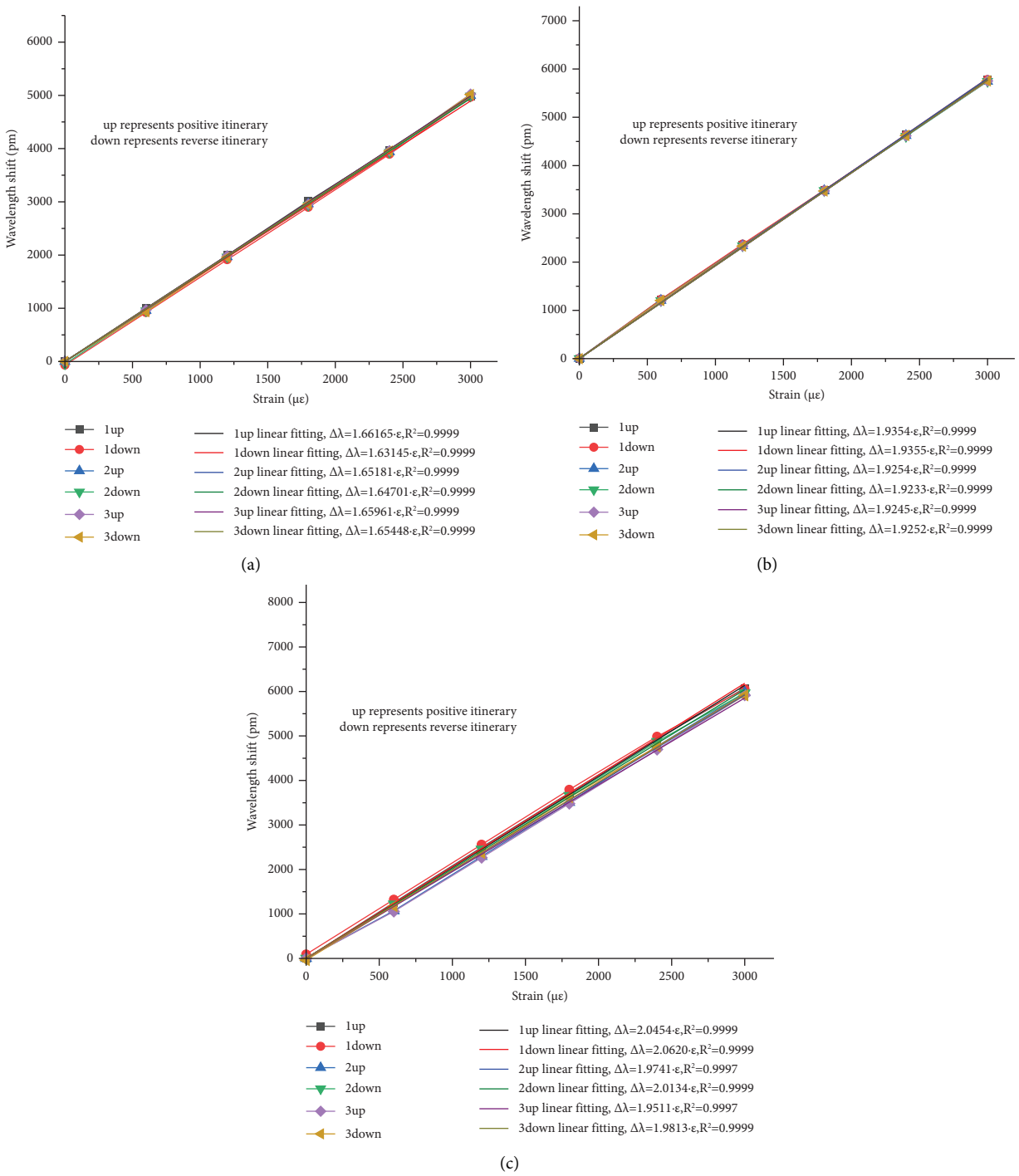

Figure 4: Fitting curves of strain sensitivity coefficient $K_{\varepsilon-S}$ for strain grating. (a) S_1 sensor, (b) S_2 sensor. (c) S_3 sensor.

$$\sigma_n = \sqrt{\frac{1}{2}\sum_{m=1}^{3}\left(\Delta\lambda_{R-\mathrm{mn}} - \Delta\overline{\lambda}_{R-n}\right)^2}. \tag{13}$$

Combined with the data in Figure 6 and equation (13), the standard deviation of the sensitivity repeatability of the sensor at each strain level can be obtained, as shown in Table 5.

The equation for the sensitivity repeatability error is as follows:

$$\gamma_R = \pm\frac{\alpha\Delta\sigma_{n,\max}}{\Delta\overline{\lambda}_{\max} - \Delta\overline{\lambda}_{\min}} \times 100\%. \tag{14}$$

Combined with Tables 4 and 5, the maximum standard deviation is $\Delta\sigma_{n,\max} = 22.036$ pm; $\Delta\overline{\lambda}_{\max} - \Delta\overline{\lambda}_{\min} = 5758.53$ pm when the confidence probability is 99.7%, the confidence

Table 3: Strain sensitivity $K_{\varepsilon-S}$.

Sensor number	Positive itinerary	Reverse itinerary	Experimental value of sensitivity coefficient $K_{\varepsilon-S,M}$ (pm/$\mu\varepsilon$)	Theoretical value of sensitivity coefficient $K_{\varepsilon-S,B}$ (pm/$\mu\varepsilon$)	Error $K_{\varepsilon-S,M} - K_{\varepsilon-S,B}/K_{\varepsilon-S,B}$ (%)
S_1	$\Delta\lambda = 1.6617 \cdot \varepsilon$ $\Delta\lambda = 1.6518 \cdot \varepsilon$ $\Delta\lambda = 1.6596 \cdot \varepsilon$	$\Delta\lambda = 1.6315 \cdot \varepsilon$ $\Delta\lambda = 1.6470 \cdot \varepsilon$ $\Delta\lambda = 1.6545 \cdot \varepsilon$	1.651	1.686	−2.08
S_2	$\Delta\lambda = 1.9354 \cdot \varepsilon$ $\Delta\lambda = 1.9254 \cdot \varepsilon$ $\Delta\lambda = 1.9245 \cdot \varepsilon$	$\Delta\lambda = 1.9355 \cdot \varepsilon$ $\Delta\lambda = 1.9233 \cdot \varepsilon$ $\Delta\lambda = 1.9252 \cdot \varepsilon$	1.928	1.926	0.10
S_3	$\Delta\lambda = 2.0454 \cdot \varepsilon$ $\Delta\lambda = 1.9741 \cdot \varepsilon$ $\Delta\lambda = 1.9511 \cdot \varepsilon$	$\Delta\lambda = 2.0620 \cdot \varepsilon$ $\Delta\lambda = 2.0134 \cdot \varepsilon$ $\Delta\lambda = 1.9813 \cdot \varepsilon$	2.005	2.107	−4.84

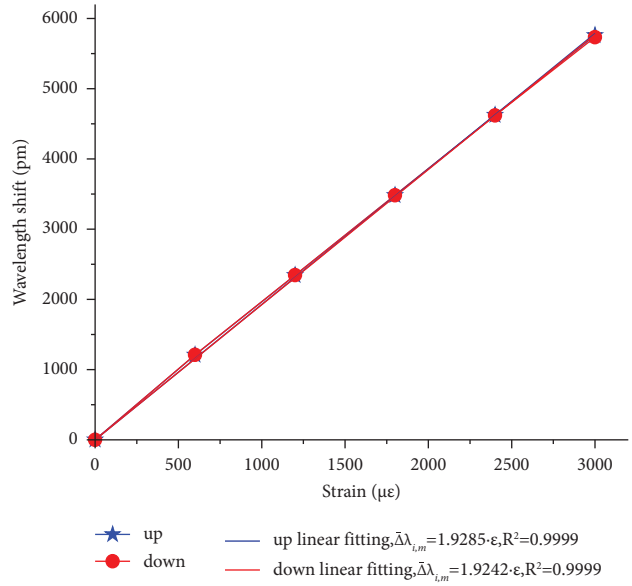

Figure 5: Fitting curves of strain grating $\Delta\bar{\lambda}_i$.

Table 4: Linearity error analysis of the strain sensitivity coefficient $K_{\varepsilon-S}$.

Path	Strain ($\mu\varepsilon$)	$\Delta\bar{\lambda}_{i,m}$ (pm)	$\Delta\bar{\lambda}_i$ (pm)	$\Delta\bar{\lambda}_i - \Delta\bar{\lambda}_{i,m}$ (pm)
Positive itinerary	0	0	1.40	1.40
	600	1157.10	1209.17	52.07
	1200	2314.20	2343.60	29.40
	1800	3471.30	3482.07	10.77
	2400	4628.40	4625.20	−3.20
	3000	5785.50	5759.20	−26.30
Reverse itinerary	3000	5772.6	5759.20	−13.40
	2400	4618.08	4619.97	1.89
	1800	3463.56	3481.90	18.34
	1200	2309.04	2346.13	37.09
	600	1154.52	1210.87	56.35
	0	0	0.67	0.67

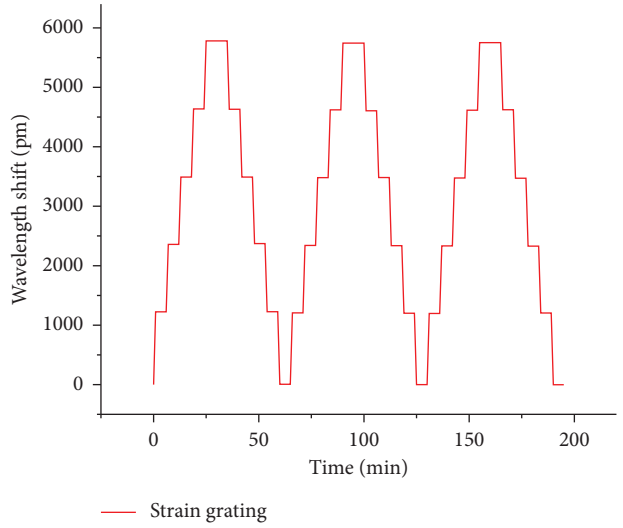

Figure 6: Wavelength shift-time curve for three repetitions of the sensor.

Table 5: Standard deviation analysis of the strain sensitivity coefficient $K_{\varepsilon-S}$.

Strain ($\mu\varepsilon$)	σ_n (pm)	
	Positive itinerary	Reverse itinerary
0	3.051	3.742
600	14.185	13.414
1200	13.028	22.036
1800	8.361	9.896
2400	11.098	13.299
3000	19.314	19.314

coefficient $\alpha = 3$, and the sensitivity repeatability error $\gamma_R = 1.15\%$ can be obtained by substituting it into formula (14), indicating that the FBG strain sensor has good stability.

4.2.3. Hysteresis Analysis of the Strain Sensitivity Coefficient $K_{\varepsilon-S}$. The hysteresis of the FBG sensor strain sensitivity is mainly caused by the sensor material and the fixed condition of the support, which reflects the degree of error between the wavelength changes of different paths corresponding to the same strain level when the sensitivity calibration is the full range output, i.e., the maximum difference between the forward and reverse strokes at the same strain is analyzed against the full range output value. The smaller the hysteresis error, the higher the monitoring accuracy.

Let the wavelength shift of the positive and reverse itinerary corresponding to each level of strain is the average value $\Delta\overline{\lambda}_{\mathrm{pi}}$ and $\Delta\overline{\lambda}_{\mathrm{ri}}$ of the three repeated test values, where $i = 1 \sim 6$. Based on Table 4, the hysteresis error analysis data are shown in Table 6.

Assuming that $\Delta\overline{\lambda}_{\mathrm{pi}}$ and $\Delta\overline{\lambda}_{\mathrm{ri}}$ corresponding to the maximum strain $3000\,\mu\varepsilon$ are $\Delta\overline{\lambda}_{p,\max}$ and $\Delta\overline{\lambda}_{r,\max}$, respectively, and $\Delta\overline{\lambda}_{\mathrm{pi}}$ and $\Delta\overline{\lambda}_{\mathrm{ri}}$ corresponding to the minimum strain $0\,\mu\varepsilon$ are $\Delta\overline{\lambda}_{p,\min}$ and $\Delta\overline{\lambda}_{r,\min}$, respectively, then the sensitivity hysteresis error can be expressed as follows:

$$\gamma_d = \pm \frac{\max\left(\Delta\overline{\lambda}_{\mathrm{pi}} - \Delta\overline{\lambda}_{\mathrm{ri}}\right)}{\max\left(\Delta\overline{\lambda}_{p,\max} - \Delta\overline{\lambda}_{p,\min}, \Delta\overline{\lambda}_{r,\max} - \Delta\overline{\lambda}_{r,\min}\right)} \times 100\%. \tag{15}$$

It can be seen from the data in Table 6 that $\max(\Delta\overline{\lambda}_{\mathrm{pi}} - \Delta\overline{\lambda}_{\mathrm{ri}}) = 5.23$ pm, $\max(\Delta\overline{\lambda}_{p,\max} - \Delta\overline{\lambda}_{p,\min}, \Delta\overline{\lambda}_{r,\max} - \Delta\overline{\lambda}_{r,\min}) = 5758.53$ pm, and the sensitivity hysteresis error $\gamma_d = 0.09\%$ can be obtained by substituting it into equation (15), indicating that the FBG strain sensor has high monitoring accuracy.

4.3. Temperature compensation Characteristic of FBG Strain Sensor

4.3.1. Calibration Test of Temperature Sensitivity Coefficients K_{T-S} and $K_{T-\mathrm{T}}$ of Strain and Temperature Compensated Grating. The S_2 sensor is selected to calibrate the temperature sensitivity coefficient. The initial center wavelength of the strain grating is 1543.6654 nm, and the initial center wavelength of the temperature grating is 1535.4299 nm. By theoretical calculation, $K_{T-S} = 28.359$pm/°C, and $K_{T-T} = 28.207$ pm/°C. The strain grating and the temperature compensation grating on the strain sensor are recorded as FBG_ε and FBG_T, respectively. The calibration test steps for the temperature sensitivity coefficient are as follows:

Table 6: Hysteresis error analysis of the strain sensitivity coefficient $K_{\varepsilon-S}$.

Strain ($\mu\varepsilon$)	$\Delta\overline{\lambda}_{\mathrm{pi}}$ (pm)	$\Delta\overline{\lambda}_{\mathrm{ri}}$ (pm)	$\Delta\overline{\lambda}_{\mathrm{pi}} - \Delta\overline{\lambda}_{\mathrm{ri}}$ (pm)
0	1.40	0.67	0.73
600	1209.17	1210.87	−1.70
1200	2343.60	2346.13	−2.53
1800	3482.07	3481.90	0.17
2400	4625.20	4619.97	5.23
3000	5759.20	5759.20	0

(1) The strain sensor is put into a heating vessel filled with pure water, and the fiber grating demodulator is connected to a jumper. (2) The initial temperature of the water is set to 20°C, and the temperature gradually increased to 70°C with an increment of 10°C *e*. At the same time, a thermometer is used to measure whether the water temperature is consistent with the indication of the thermostatic bath to avoid reading errors. During the period, the FBG_ε and FBG_T center wavelength readings corresponding to the demodulator are recorded by the software system. (3) cooling to 20°C at a rate of 10°C per stage; the process is the same as (2), forming a cycle; (4) Repeat steps (2)~(3) twice. The accuracy of the thermostat vessel used in the experiment is 0.001°C, the accuracy of the thermometer is 0.1°C, and the wavelength resolution of the fiber grating demodulator is 0.1 pm. The device is shown in Figure 7.

Taking the drift $\Delta\lambda$ of the central wavelength of each level of the grating relative to the initial central wavelength as the vertical coordinate and the temperature variation ΔT as the horizontal coordinate, the diagram is drawn and linearly fitted. The test results are shown in Figures 8 and 9.

As it can be seen from Figures 8 and 9, the wavelength shifts $\Delta\lambda$ of the two gratings is positively correlated with the temperature variation ΔT, with a linear correlation coefficient of 99.97% or more. The slope of the linear fitting curve is the temperature sensitivity coefficients K_{T-S} and K_{T-T} of the FBG strain sensor. The average value of the temperature sensitivity coefficients of the six positive and reverse itineraries was taken as the test values $K_{T-S,M}$ and $K_{T-T,M}$ of the strain sensitivity coefficients of the sensor and compared with their theoretical values, and the compiled data are shown in Table 7.

From Table 7, the temperature sensitivity coefficient of this FBG sensor has a small error with its theoretical values of −0.79% and 0.29%, respectively.

To further verify the performance of the two gratings of the FBG strain sensor when the temperature changes, the linearity, repeatability, and hysteresis of the temperature sensitivity coefficients K_{T-S} and K_{T-T} of the strain grating and the temperature-compensated grating of the sensor are examined with reference to Section 4.2.1–4.2.3. The corresponding errors of K_{T-S} are −0.92%, 1.13% and 0.45%, respectively. For K_{T-T}, the values are −0.91%, 1.15%, and −0.23%, respectively. The analysis results show that the

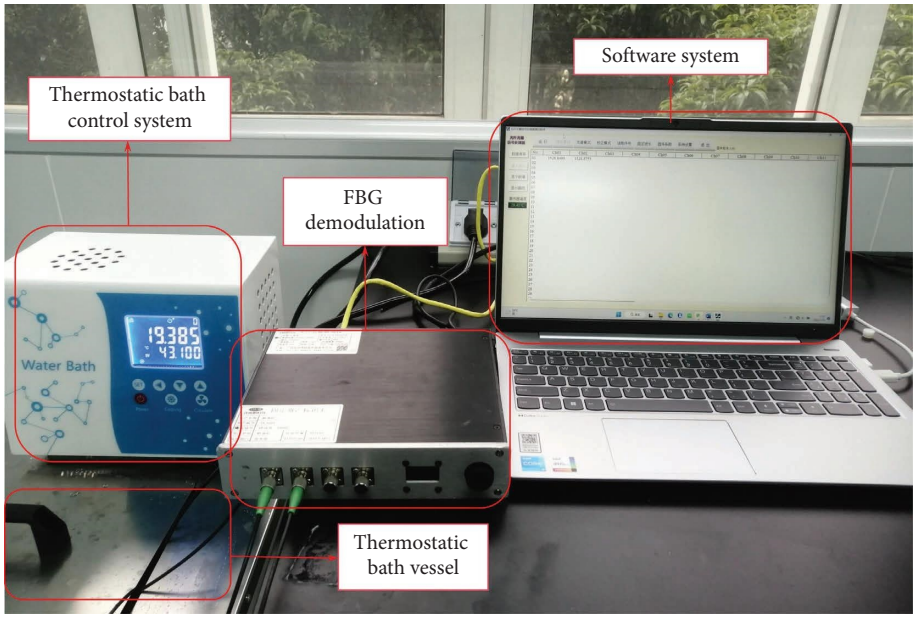

Figure 7: Temperature compensation test device.

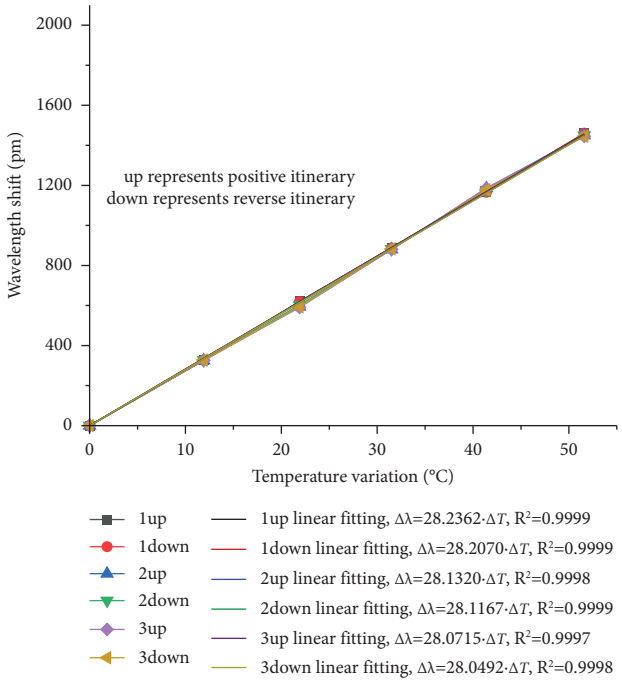

Figure 8: Fitting curves for temperature sensitivity K_{T-S}.

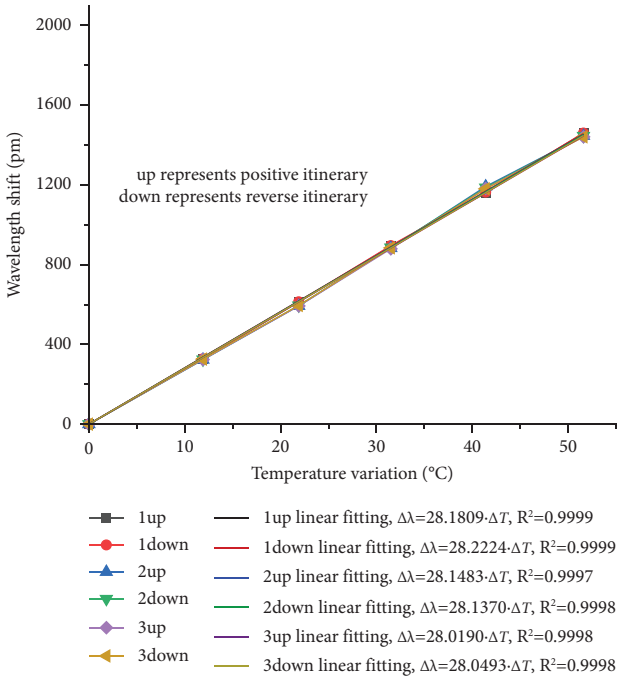

Figure 9: Fitting curves for temperature sensitivity K_{T-T}.

strain performance of the two gratings is excellent when the temperature changes.

4.3.2. Temperature compensation Validation Test. To verify the accuracy of strain monitoring of the FBG strain sensor under different temperature environments, the temperature in the constant temperature chamber was increased to 40°C (i.e., 20°C higher than the temperature when $K_{\varepsilon-S}$ was calibrated). The FBG strain sensor was loaded and unloaded at all strain levels according to the calibration process of $K_{\varepsilon-S}$ in Section 4.2, and the central wavelength changes of the strain grating and the temperature grating under each level of strain were recorded and compared.

According to equation (11), when the FBG strain sensor is subjected to both temperature and axial force, its strain due to axial force can be expressed as follows:

$$\varepsilon = \frac{\Delta\lambda_B - K_{T-S}\left(\Delta\lambda_{B,T}/K_{T-T}\right)}{K_{\varepsilon-S}}, \tag{16}$$

Table 7: Temperature sensitivity coefficients K_{T-S} and K_{T-T}.

Grating	Positive itinerary	Reverse itinerary	Experimental value of sensitivity coefficient $K_{T-,M}$ (pm/°C)	Theoretical value of sensitivity coefficient $K_{T-,B}$ (pm/°C)	Error $(K_{T-,M} - K_{T-,B}/K_{T-,B})$ (%)
FBG_ε	$\Delta\lambda = 28.2362 \cdot \Delta T$ $\Delta\lambda = 28.1320 \cdot \Delta T$ $\Delta\lambda = 28.0715 \cdot \Delta T$	$\Delta\lambda = 28.2070 \cdot \Delta T$ $\Delta\lambda = 28.1167 \cdot \Delta T$ $\Delta\lambda = 28.0492 \cdot \Delta T$	28.135	28.359	−0.79
FBG_T	$\Delta\lambda = 28.1809 \cdot \Delta T$ $\Delta\lambda = 28.1483 \cdot \Delta T$ $\Delta\lambda = 28.0190 \cdot \Delta T$	$\Delta\lambda = 28.2224 \cdot \Delta T$ $\Delta\lambda = 28.1370 \cdot \Delta T$ $\Delta\lambda = 28.0493 \cdot \Delta T$	28.126	28.207	−0.29

Table 8: Error analysis for all levels of strain after temperature compensation.

Path	Strain ε_S ($\mu\varepsilon$)	$\Delta\lambda_B$ (pm)	$\Delta\lambda_{B,T}$ (pm)	ε_T ($\mu\varepsilon$)	Absolute error of strain $\varepsilon_T - \varepsilon_S$ (pm)	Relative error of strain $(\varepsilon_T - \varepsilon_S/\varepsilon_S)$ (%)
Positive itinerary	600	1757.90	558.90	621.80	21.80	3.63
	1200	2936.70	560.20	1232.48	32.48	2.71
	1800	4104.30	559.60	1838.39	38.39	2.13
	2400	5309.90	560.30	2463.34	63.34	2.64
	3000	6485.00	558.60	3073.72	73.72	2.46
Reverse itinerary	3000	6485.00	558.60	3073.72	73.72	2.46
	2400	5288.60	559.50	2452.71	52.71	2.20
	1800	4110.90	558.30	1842.49	42.49	2.36
	1200	2946.40	559.20	1238.03	38.03	3.17
	600	1768.60	559.90	626.78	26.78	4.46

where $\Delta\lambda_B$ is the difference between the center wavelength of the strain grating at all strain levels at the validation test room temperature of 40°C and the center wavelength at zero strain at the strain calibration test room temperature of 20°C. $\Delta\lambda_{B,T}$ is the difference between the center wavelength of the temperature-compensated grating at the validation test room temperature of 40°C and the center wavelength at the strain calibration test room temperature of 20°C. The coefficients $K_{\varepsilon-S}$, K_{T-S}, and K_{T-T} are taken from the calibrated test values and are 1.928 pm/$\mu\varepsilon$, 28.135 pm/$\mu\varepsilon$, and 28.126 pm/$\mu\varepsilon$, respectively. The initial center wavelengths of the strain grating and temperature-compensated grating for the strain calibration were 1543.6654 nm and 1535.4299 nm, respectively. The experimental data are listed in Table 8.

The strain ε_S in Table 8 represents the strain values at all levels, which is also the actual strain of the FBG sensor; ε_T is based on the measured data in equation (16) to calculate the strain of the sensor monitored by the strain grating after temperature compensation. From the analysis results, it can be seen that the errors at all levels of strain are positive values, which means the test monitoring value after temperature compensation is greater than the real strain. The reason may be caused by the structure of the sensor itself. Because the temperature compensation grating is bonded to the clamping rod of stainless steel, the actual temperature may be greater than the temperature of the strain grating suspended in the spring, so the compensated strain is slightly larger, but the error is within 5%. This indicates that the temperature reference grating method can be used to compensate for the strain due to temperature in the FBG sensor in the presence of both temperature and stress, thus accurately monitoring the strain due to stress and providing accurate strain monitoring data for the test object.

According to the test results in Sections 4.2 and 4.3, the performance of the FBG strain sensor developed in this paper is further compared with the conventional ones, as shown in Table 9. As can be seen from the table, the FBG strain sensor developed in this paper realizes adjustable sensitivity and temperature compensation, and a series of tests and quantitative analysis are carried out on the linearity, repeatability, and hysteresis performance of its sensitivity, which provides flexible monitoring means and technical support for different complex engineering structures and their various components.

Table 9: Comparison of the performance of FBG strain sensors developed in this paper with conventional FBG strain sensors.

Items	Strain sensitivity $K_{\varepsilon-S}$ adjustable?	The linearity error of $K_{\varepsilon-S}$	The repeatability error of $K_{\varepsilon-S}$	The hysteresis error of $K_{\varepsilon-S}$	Temperature compensation?	Temperature compensation verification?
Li et al. [34]	No	Unanalyzed	0.41% and 1.21%	0.37% and 0.86%	Yes	No
Nawrot et al. [31]	No	Unanalyzed	Unanalyzed	Unanalyzed	No	No
Li et al. [28]	No	Unanalyzed	Less than 0.50%	Unanalyzed	No	No
Peng et al. [30]	No	No clear data	No clear data	No clear data	No	No
This paper	Yes	0.98%	1.15%	0.09%	Yes	Yes, and the maximum error is 4.46%

5. Conclusions

In this paper, a new sensitivity adjustable FBG strain sensor is designed, its strain sensing algorithm and temperature compensation algorithm are theoretically and experimentally investigated, and the following conclusions are reached:

(1) The strain sensitivity of the strain sensor is adjusted to meet the monitoring requirements of different engineering structures by adjusting the ratio of the distance between the midpoint of the two fixed tubes and the distance between the paste points at the two ends of the grating, i.e., the value of L/L_{FBG}. In the calibration test, the strain sensitivity test value was within ±5% of the theoretical value, and its linearity, repeatability, and hysteresis were less than 1.2%, indicating excellent strain performance.

(2) Further temperature compensation verification tests were carried out on the sensor, and when the temperature difference was 20°C, the error between the monitored strain and the actual strain was within 5% after correction by temperature compensation. This FBG strain sensor can meet the needs of different engineering structures for strain monitoring and provides reliable data acquisition.

(3) The temperature sensitivity coefficients of the strain grating and temperature-compensated grating of the FBG sensor were calibrated, and the error between the test value and the theoretical value of the two grating temperature sensitivity coefficients was within ±1%, and their linearity, repeatability, and hysteresis were less than 1.2%, indicating their excellent temperature performance.

(4) The temperature compensation equation was derived based on the temperature reference grating method, and a temperature compensation verification test was carried out at a temperature difference of 20°C. The analysis results showed that the error between the monitored strain and the actual strain was within 5% at all strain levels, indicating that the temperature reference grating method can compensate well for the strain generated by temperature, thus providing reliable monitoring data for the analysis of the internal force of the structure under the coupling effect of force and temperature.

Data Availability

The data used to support the findings of this study are available from the corresponding author upon request.

Conflicts of Interest

The authors declare that there are no conflicts of interest.

Acknowledgments

This work was supported by the Natural Science Foundation of China (Grant no. 52068014), Key R&D Projects in the Guangxi Autonomous Region (Grant no. GUIKE AA20302006), and Hunan Provincial Department of Transportation Science and Technology Plan Project (Grant no. 202015).

References

[1] E. Aytulun and S. Soyöz, "Implementation and application of a SHM system for tall buildings in Turkey," *Bulletin of Earthquake Engineering*, vol. 20, no. 9, pp. 4321–4344, 2022.

[2] P. Cawley, "Structural health monitoring: closing the gap between research and industrial deployment," *Structural Health Monitoring*, vol. 17, no. 5, pp. 1225–1244, 2018.

[3] C. Fang, Y. L. Xu, R. Hu, and Z. Huang, "A web-based and design-oriented structural health evaluation system for long-span bridges with structural health monitoring system," *Structural Control and Health Monitoring*, vol. 29, no. 2, p. e2879, 2022.

[4] P. F. Giordano, S. Quqa, and M. P. Limongelli, "The value of monitoring a structural health monitoring system," *Structural Safety*, vol. 100, Article ID 102280, 2023.

[5] Z. He, W. Li, H. Salehi, H. Zhang, H. Zhou, and P. Jiao, "Integrated structural health monitoring in bridge engineering," *Automation in Construction*, vol. 136, Article ID 104168, 2022.

[6] D. Anastasopoulos, E. P. Reynders, S. François et al., "Vibration-based monitoring of an FRP footbridge with embedded fiber-Bragg gratings: influence of temperature vs.damage," *Composite Structures*, vol. 287, Article ID 115295, 2022.

[7] S. Goossens, F. Berghmans, K. Muñoz et al., "A global assessment of barely visible impact damage for CFRP subcomponents with FBG-based sensors," *Composite Structures*, vol. 272, Article ID 114025, 2021.

[8] J. Kumar, G. Singh, M. K. Saxena, O. Prakash, S. K. Dixit, and S. V. Nakhe, "Development and studies on FBG temperature sensor for applications in nuclear fuel cycle facilities," *IEEE Sensors Journal*, vol. 21, no. 6, pp. 7613–7619, 2021.

[9] H. Kwon, Y. Park, J. H. Kim, and C. G. Kim, "Embedded fiber Bragg grating sensor–based wing load monitoring system for composite aircraft," *Structural Health Monitoring*, vol. 18, no. 4, pp. 1337–1351, 2019.

[10] S. Takeda, M. Sato, and T. Ogasawara, "Simultaneous measurement of strain and temperature using a tilted fiber Bragg grating," *Sensors and Actuators A: Physical*, vol. 335, Article ID 113346, 2022.

[11] B. Van Esbeen, C. Finet, R. Vandebrouck et al., "Smart railway traffic monitoring using fiber bragg grating strain gauges," *Sensors*, vol. 22, no. 9, p. 3429, 2022.

[12] M. Fisser, R. A. Badcock, P. D. Teal, and A. Hunze, "High-sensitivity fiber-optic sensor for hydrogen detection in gas and transformer oil," *IEEE Sensors Journal*, vol. 19, no. 9, pp. 3348–3357, 2019.

[13] M. A. Alias, M. F. Ismail, M. S. M. Sa'ad et al., "A high-precision extensometer system for ground displacement

measurement using fiber bragg grating," *IEEE Sensors Journal*, vol. 22, no. 9, pp. 8509–8521, 2022.

[14] J. Braunfelds, U. Senkans, P. Skels et al., "Road pavement structural health monitoring by embedded fiber-bragg-grating-based optical sensors," *Sensors*, vol. 22, no. 12, p. 4581, 2022.

[15] K. Al Handawi, N. Vahdati, P. Rostron, L. Lawand, and O. Shiryayev, "Strain based FBG sensor for real-time corrosion rate monitoring in pre-stressed structures," *Sensors and Actuators B: Chemical*, vol. 236, pp. 276–285, 2016.

[16] O. Almubaied, H. K. Chai, M. R. Islam, K. S. Lim, and C. G. Tan, "Monitoring corrosion process of reinforced concrete structure using FBG strain sensor," *IEEE Transactions on Instrumentation and Measurement*, vol. 66, no. 8, pp. 2148–2155, 2017.

[17] A. H. Poh, M. R. A. Hassan, M. H. A. Bakar, F. R. M. Adikan, and M. Moghavvemi, "Profile morphology of fiber Bragg gratings during initial cracking: a case study on proof load testing of an arch spandrel segment," *IEEE Sensors Journal*, vol. 22, no. 6, pp. 5678–5687, 2022.

[18] J. Alvarez-Montoya, A. Carvajal-Castrillón, and J. Sierra-Pérez, "In-flight and wireless damage detection in a UAV composite wing using fiber optic sensors and strain field pattern recognition," *Mechanical Systems and Signal Processing*, vol. 136, Article ID 106526, 2020.

[19] O. S. Bursi, N. Tondini, M. Fassin, and A. Bonelli, "Structural monitoring for the cyclic behaviour of concrete tunnel lining sections using FBG sensors," *Structural Control and Health Monitoring*, vol. 23, no. 4, pp. 749–763, 2016.

[20] P. Velha, T. Nannipieri, A. Signorini et al., "Monitoring large railways infrastructures using hybrid optical fibers sensor systems," *IEEE Transactions on Intelligent Transportation Systems*, vol. 21, no. 12, pp. 5177–5188, 2020.

[21] W. Zhu, Q. Shen, and H. Qin, "Research and application of FBG monitoring technology in internal prestressed steel strand," *Acta Photonica Sinica*, vol. 48, no. 2, pp. 68–75, 2019.

[22] S. Sridevi, K. S. Vasu, S. Asokan, and A. K. Sood, "Enhanced strain and temperature sensing by reduced graphene oxide coated etched fiber Bragg gratings," *Optics Letters*, vol. 41, no. 11, pp. 2604–2607, 2016.

[23] R. Oliveira, L. Bilro, T. H. Marques, C. M. Cordeiro, and R. Nogueira, "Strain sensitivity enhancement of a sensing head based on ZEONEX polymer FBG in series with silica fiber," *Journal of Lightwave Technology*, vol. 36, no. 22, pp. 5106–5112, 2018.

[24] S. W. Kim, M. C. Cha, I. Lee, E. H. Kim, I. B. Kwon, and T. K. Hwang, "Damage evaluation and strain monitoring of composite plates using metal-coated FBG sensors under quasi-static indentation," *Composites Part B: Engineering*, vol. 66, pp. 36–45, 2014.

[25] S. Sridhar, S. Sebastian, A. K. Sood, and S. Asokan, "A study on MoS_z nanolayer coated etched fiber Bragg grating strain sensor," *IEEE Sensors Journal*, vol. 21, no. 7, pp. 9171–9178, 2021.

[26] M. Ghimire, C. Wang, K. Dixon, and M. Serrato, "In situ monitoring of prestressed concrete using embedded fiber loop ringdown strain sensor," *Measurement*, vol. 124, pp. 224–232, 2018.

[27] V. P. Matveenko, I. N. Shardakov, A. A. Voronkov et al., "Measurement of strains by optical fiber Bragg grating sensors embedded into polymer composite material," *Structural Control and Health Monitoring*, vol. 25, no. 3, p. e2118, 2018.

[28] R. Li, Y. Chen, Y. Tan, Z. Zhou, T. Li, and J. Mao, "Sensitivity enhancement of FBG-based strain sensor," *Sensors*, vol. 18, no. 5, p. 1607, 2018.

[29] M. Liu, W. Wang, H. Song, S. Zhou, and W. Zhou, "A high sensitivity FBG strain sensor based on flexible hinge," *Sensors*, vol. 19, no. 8, p. 1931, 2019.

[30] J. Peng, S. Jia, Y. Jin, S. Xu, and Z. Xu, "Design and investigation of a sensitivity-enhanced fiber Bragg grating sensor for micro-strain measurement," *Sensors and Actuators A: Physical*, vol. 285, pp. 437–447, 2019.

[31] U. Nawrot, T. Geernaert, B. De Pauw et al., "Development of a mechanical strain amplifying transducer with Bragg grating sensor for low-amplitude strain sensing," *Smart Materials and Structures*, vol. 26, no. 7, Article ID 75006, 2017.

[32] S. J. Jeon, S. Y. Park, and S. T. Kim, "Temperature compensation of fiber Bragg grating sensors in smart strand," *Sensors*, vol. 22, no. 9, p. 3282, 2022.

[33] A. Leal-Junior, A. Frizera, C. Díaz, C. Marques, M. Ribeiro, and M. J. Pontes, "Material features based compensation technique for the temperature effects in a polymer diaphragm-based FBG pressure sensor," *Optics Express*, vol. 26, no. 16, pp. 20590–20602, 2018.

[34] R. Li, Y. Tan, Y. Chen, L. Hong, and Z. Zhou, "Investigation of sensitivity enhancing and temperature compensation for fiber Bragg grating (FBG)-based strain sensor," *Optical Fiber Technology*, vol. 48, pp. 199–206, 2019.

[35] G. F. Pérez-García, J. L. Camas-Anzueto, G. Anzueto-Sánchez, M. Pérez-Patricio, and F. R. López-Estrada, "Demonstration of improving the sensitivity of a fiber optic temperature sensor using the wavelength of maximum absorption of the lophine," *Measurement*, vol. 187, Article ID 110378, 2022.

[36] L. Xiong, G. Jiang, Y. Guo, Y. Kuang, and H. Liu, "Investigation of the temperature compensation of FBGs encapsulated with different methods and subjected to different temperature change rates," *Journal of Lightwave Technology*, vol. 37, no. 3, pp. 917–926, 2019.

[37] K. O. Hill and G. Meltz, "Fiber Bragg grating technology fundamentals and overview," *Journal of Lightwave Technology*, vol. 15, no. 8, pp. 1263–1276, 1997.

[38] H. Xu, X. Zheng, W. Zhao et al., "High precision, small size and flexible FBG strain sensor for slope model monitoring," *Sensors*, vol. 19, no. 12, p. 2716, 2019.

[39] H. Wu, Q. Lin, Z. Jiang, F. Zhang, L. Li, and L. Zhao, "A temperature and strain sensor based on a cascade of double fiber Bragg grating," *Measurement Science and Technology*, vol. 30, no. 6, Article ID 065104, 2019.

[40] H. Qin, W. Zhu, H. Zhang, Z. Zhou, and J. Ou, "Manufacturing and performance analysis of intelligent steel strand embedded with prepressure large scale fiber bragg grating sensor," *Chinese Journal of Lasers*, vol. 44, no. 4, pp. 216–223, 2017.